Large Eddy Simulation of a turbulent non-premixed propane-air reacting flame in a cylindrical combustor

S. C. Paul [a,1] M. C. Paul [a,*] W. P. Jones [b]

[a] *Department of Mechanical Engineering, University of Glasgow, Glasgow G12 8QQ, UK*

[b] *Department of Mechanical Engineering, Imperial College London, Exhibition Road, London SW7 2AZ, UK*

Abstract

Large Eddy Simulation (LES) is applied to investigate the turbulent non-premixed combustion flow, including species concentrations and temperature, in a cylindrical combustor. Gaseous propane (C_3H_8) is injected through a circular nozzle which is attached at the centre of the combustor inlet. Preheated air with a temperature of $773K$ is supplied through the annulus surrounding of this fuel nozzle. In LES a spatial filtering is applied to the governing equations to separate the flow field into large-scale and small-scale eddies. The large-scale eddies which carry most of the turbulent energy are resolved explicitly, while the unresolved small-scale eddies are modelled using the Smagorinsky model with $C_s = 0.1$ as well as dynamically calibrated C_s. The filtered values of the species mass fraction, temperature and density, which are the functions of the mixture fraction (conserved scalar), are determined by integration over a beta Probability Density Function (β-PDF). The computational results are compared with those of the experimental investigation conducted

by Nishida and Mukohara [1]. According to this experiment, the overall equivalence ratio of 0.6, which is calculated from the ratio of the air flow rate supplied to the combustion chamber to that of the stoichiometric reaction, is kept constant so that the turbulent combustion at the fuel nozzle exit starts under the fuel-rich conditions.

Key words: Large Eddy Simulation, Turbulent flow, Non-premixed combustion

1 Introduction

Turbulent non-premixed combustion occurs in many engineering applications. An understanding of turbulent combustion processes is essential for the efficient design of many engineering devices such as gas turbines, internal combustions engines, furnaces etc. Moreover, the number of combustion systems used in the transformation and transportation industries is growing rapidly, and as a result, a large amount of combustion products such as NO_x, CO and unburned hydrocarbons, which are harmful to human health and a great threat to the global environment, are produced everyday. The accurate control and prediction of a turbulent flame and the increment of the combustion efficiency, therefore, appear to be an important and essential part in combustion engineering.

Combustion remains one of the most complicated phenomena to describe and simulate using numerical tools, mainly because a practical combustion process is usually involves turbulent flow. The multi-scale character of turbulence

* Corresponding author: Tel:+44 (0)141 330 8466, Fax:+44 (0)141 330 4343.
Email address: m.paul@mech.gla.ac.uk (M. C. Paul).
[1] Present Address: BRE Centre for Fire Safety Engineering, School of Engineering, The University of Edinburgh, Mayfield Road, Edinburgh EH9 3JL, UK.

makes the simulation of such flow a difficult task. In order to account rigorously for the full nonlinear effects of turbulence in a combustion process, the governing equations are solved numerically such that the finest turbulence scales, known as *Kolmogorov scales*, must be resolved. However, to date this is a very difficult and computationally demanding task for a practical system. Thus, depending on the scale of interest, different techniques with different modelling approaches exist in the literature. Large Eddy Simulation (LES) is one of them and has recently been shown to be a promising approach for the computation of turbulent flows, because of its clear means of overcoming some of the deficiencies which appear in other available approaches such as Reynolds Averaged Navier Stokes (RANS) and Direct Numerical Simulation (DNS) which is restricted to low Reynolds number flows.

In the traditional RANS approach, the governing equations of motion are either time or ensemble averaged, which produces unknown quantities, known as the Reynolds stresses after the early work done by Reynolds [2]. These unknown stresses then have to be modelled before solution of the equations is possible. There are various modelling techniques available in the literature, though as the governing equations are averaged, it is only possible to predict the behaviour of the averaged (mean) values of the flow variables. On the other hand, DNS resolves all turbulence scales present in a flow and the approach is essentially model free. Thus, with DNS it might be possible to compute the instant profiles of all the flow variables, but as mentioned, it is feasible only in a flow with low Reynolds numbers. In most practical engineering flows, such as one considered in this paper, the Reynolds number is high, and an application of DNS to compute those turbulent flows becomes impractical, given the computational capability available at present. Even with a rapidly increasing

computing power this is likely to remain the situation for many years. A review work dealing the current status of DNS applied to non-premixed combustion is done by Vervisch and Poinsot [3].

In LES, a spatial filtering approach is applied to the governing equations in order to filter out the sub-grid scale (sgs) motions from the large scale. The large scale motions which carry most of the turbulent energy are resolved explicitly, while the unresolved smaller scales are modelled. A suitably defined filter function of width proportional to the mesh spacing of the numerical scheme is usually selected. The chemical reactions that control combustion, however, occur at the smallest scales of the flow and can almost never be fully resolved. As such, modelling approaches are needed in order to predict accurately the chemical behaviour of reacting flows, e.g. pdf approaches. Regarding the modelling of the sub-grid scale (sgs) eddies, the majority of LES applications have utilised the eddy viscosity approach formulated first by Smagorinsky [4] and developed further by Lilly [5]. The ideas were further developed by Deardorff [6] who simulated a plane Poiseuille flow (channel flow), which represents one of the earliest applications of LES in the area of engineering. Since then, LES has been developed by a large number of researchers and applied to a range of increasingly complex problems, such as LES of turbulent confined co-annular jets, Akselvoll and Moin [7], LES of a plane jet in a cross-flow, Jones and Wille [8], LES of a round jet in a cross flow, Yuan et al. [9], and LES of turbulent flow past a swept fence, di Mare and Jones [10]. Comprehensive reviews on Large eddy Simulation of turbulent flows can be found in Lesieur and Metais [11], Moin [12] and Lesieur et al. [13].

LES application to turbulent reacting flows began in the 1990s. Since then a number of papers have demonstrated the power of LES to the flows of tur-

bulent combustion, such as an LES scheme for turbulent reacting flows of Gao and O'Brien [14], LES of a non-premixed reacting jet, DesJardin and Frankel [15], LES of a turbulent non-premixed flame, Branley and Jones [16], LES of a model gas turbine combustor, di Mare et al.[17] and LES of auto-ignition, [18; 19]. Peters [20], Pitsch [21] and Riley [22] also offer a comprehensive review of Large Eddy Simulation of turbulent combustion.

In the present paper, our aim is to investigate the turbulent non-premixed combustion, including species concentrations and temperature, in a model cylindrical combustor by using LES. A schematic of the cylindrical combustor including the computational domain is shown in Fig. 1, which corresponds to the configuration investigated experimentally by Nishida and Mukohara [1]. Gaseous propane (C_3H_8) is injected through a circular nozzle with an internal diameter of $2mm$ at the centre of the combustor inlet, while the pre-heated air with an averaged velocity of $0.96ms^{-1}$ and temperature of $773K$ is supplied through the annulus of $115mm$ diameter surrounding the fuel nozzle into the $1m$ long combustion chamber. The overall equivalence ratio is maintained at 1.6 so that the burning occurs in a fuel-rich non-premixed combustion mode. The average fuel velocity of $30ms^{-1}$ was measured by [1] at the inlet, which corresponds to a flow Reynolds number of $13,000$. The presently computed temperature and species concentration fields are compared with those of the experimental investigation of Nishida and Mukohara [1]. To the best of the authors' knowledge this is the first time that the turbulent flame inside this combustion chamber under the fuel-rich condition is investigated by means of LES.

The paper is structured in the following order. A brief description of the necessary mathematical formulation in LES including the sgs modelling and

the conserved scalar approach to combustion modelling is given in §2. In §3 the computational procedure and the necessary boundary conditions used in the LES are described. Results and discussion are presented in §4. Finally, conclusions on the findings are drawn in §5.

2 Mathematical formulation in LES

To obtain the LES equations the governing equations of motions are filtered first by applying a spatial filter, a technique to separate the large scale (resolved scale) flow field from the small scale (sub-grid scale) [23]. Applying the density weighted-filtered function [24] to the continuity, Navier-Stokes and mixture fraction (conserved scalar) equations gives:

$$\frac{\partial \bar{\rho}}{\partial t} + \frac{\partial \bar{\rho}\tilde{u}_j}{\partial x_j} = 0, \tag{1}$$

$$\frac{\partial \bar{\rho}\tilde{u}_i}{\partial t} + \frac{\partial \bar{\rho}\tilde{u}_i\tilde{u}_j}{\partial x_j} = -\frac{\partial \bar{p}}{\partial x_i} + \frac{\partial}{\partial x_j}\left[2\mu\bar{S}_{ij} - \frac{2}{3}\mu\bar{S}_{kk}\delta_{ij}\right] - \frac{\partial \tau_{ij}}{\partial x_j}, \tag{2}$$

$$\frac{\partial \bar{\rho}\tilde{\xi}}{\partial t} + \frac{\partial \bar{\rho}\tilde{u}_j\tilde{\xi}}{\partial x_j} = \frac{\partial}{\partial x_j}\left(\Gamma\frac{\partial \tilde{\xi}}{\partial x_j}\right) - \frac{\partial J_j}{\partial x_j}, \tag{3}$$

where t is time; x_j is the spatial coordinate directions; u_j is the velocity vector; p is the pressure; ρ is the density, which, in reacting flows, varies due to the heat release from the chemical reaction and on the chemical composition of the fluid. μ is the molecular viscosity, $S_{ij} = \frac{1}{2}(\frac{\partial u_i}{\partial x_j} + \frac{\partial u_j}{\partial x_i})$ is the strain rate, δ_{ij} is the Kronecker delta, ξ is the conserved scalar or the mixture fraction, and $\Gamma = \frac{\mu}{Pr} = \frac{\mu}{Sc}$ is the diffusion coefficient where Pr/Sc is the Prandtl/Schmidt number.

The sub-grid scale stresses, τ_{ij}, are modelled using the eddy viscosity assumption of Smagorinsky [4]:

$$\tau_{ij} - \frac{1}{3}\delta_{ij}\tau_{kk} = -2\bar{\rho}(C_s\Delta)^2|\bar{S}|\bar{S}_{ij}, \tag{4}$$

where Δ is the filter width and $|\bar{S}| = \sqrt{2\bar{S}_{ij}\bar{S}_{ij}}$ is the magnitude of the resolved strain rate tensor, $\bar{S}_{ij}$. Two computations have been performed, one with the Smagorinsky constant, C_s, of 0.1 (Case1) as suggested by Branley and Jones [16] and another one with its dynamically calibrated values, Germano et al. [25] (Case2), clipping the negative values of C_s to zero. We also note that Jones and Wille [8] argued the value of the Smagorinsky constant of 0.23 used by Lilly [5] is too large, which could result in excessive attenuation of small scales. In other successful simulations of channel flow (e.g. Deardorff [6]), the value of Cs, for instance, was around 0.07 while the values of 0.081–0.1 were used in mixing layers by Yoshizawa [26].

For the sub-grid scale scalar flux, J_j, a gradient model, Schmidt and Schumann [27],

$$J_j = -\bar{\rho}\Gamma_{sgs}\frac{\partial\tilde{\xi}}{\partial x_j} = -\bar{\rho}\frac{(C_s\Delta)^2|\bar{S}|}{\sigma_{sgs}}\frac{\partial\tilde{\xi}}{\partial x_j}, \tag{5}$$

is applied, where σ_{sgs} is a constant sub-grid scale Prandtl/Schmidt number which is assigned a value of 0.7.

The combustion is modelled via the conserved scalar modelling approach with the laminar flamelet model, Peters [28]. In this approach, the chemical reaction rates are assumed to be fast compared to the rate at which reactants mix. The mixing is described by a strictly conserved scalar also known as the mixture fraction. The instantaneous species concentrations are then considered to be

a unique function of this conserved scalar. As the functional dependence is highly nonlinear, mean or filtered values are obtained via the probability density function of the conserved scalar [29]. Once the density weighted mixture fraction, $\tilde{\xi}$, and its sub-grid scale variance are known, the filtered density ($\bar{\rho}$) and density weighted thermochemical variables ($\tilde{\phi}$) are obtained by integrating over a β - probability density function. Further details of this model are given in Paul [30] and di Mare et al. [17].

3 Computational procedure

3.1 Grid arrangement and boundary conditions

A curvilinear body fitted coordinate system is employed for the present simulation consisting of a total of about 1.5 million nodes inside the combustion chamber with a non-uniform mesh distributed along the three co-ordinate directions. At the centre of the combustor inlet, where the fuel is injected through a circular nozzle at a speed relatively higher than that of the air supplied through the cylinder, a very fine mesh is required so that the steep gradients that appear in this area are adequately resolved. The mesh lines are contracted at the centre and near the inlet of the combustor, and they are expanded smoothly in all the three directions outwards from the centreline and inlet (Fig. 2).

In the absence of the results of the flow-field measurement (mean velocity profiles and fluctuations) in [1], we have used the one-seventh empirical power-law profile to generate the fully developed turbulent streamwise mean velocity profile at the inlet of the fuel injector. With the bulk Reynolds number of

13,000, the ratio of the bulk velocity to the mean centreline velocity becomes 0.82 which gives the centreline mean velocity of about 36.73 at the fuel inlet. A simple polynomial relation with the turbulent intensity of about 5% (estimated by using $0.16Re^{-1/8}$ but has close agreement with Durst and Unsal [31]) is fitted to the data of Laufer [32] to generate the rms profiles of the velocity fluctuations of the flow [30]. Then, the instantaneous velocity field is generated by using the Gaussian distributed noise as

$$\tilde{u}_i(x_i,t) =< \tilde{u}_i(x_i) > +\psi(x_i,t)u'_{rms} \tag{6}$$

where ψ is a Gaussian random distribution. The mixture fraction at the inlet is defined as

$$\xi = \begin{cases} 1 \text{ in the fuel stream} \\ \\ 0 \text{ in the air stream.} \end{cases} \tag{7}$$

At the outlet boundary, a non-reflective boundary condition is used, a condition sufficient to minimise the effects of the outlet boundary in the solutions. A thin viscous sub-layer develops adjacent to the walls of the combustor and a prohibitively fine mesh would be required to resolve this. To overcome this difficulty an equilibrium log-law condition is employed as a near wall condition at the surfaces of the combustor.

3.2 Numerical method

The in-house developed finite volume code LES-BOFFIN (Boundary Fitted Flow Integrator) has been used to solve the governing equations. The code is

based on a fully implicit low-Mach number formulation and is second order accurate in both space and time. The BOFFIN code has been applied extensively in the LES of reacting and non-reacting turbulent flows; for examples, see LES of a gas turbine combustor, di Mare et al.[17], of a turbulent non-premixed flame Branley and Jones [16], and of turbulent flow past a swept fence di Mare and Jones [10]. For a full details of the numerical method used in the BOFFIN, the readers are referred to those published papers and the relevant references therein.

An energy conserving discretisation [33] is used for the convective terms in the momentum equations (2), while all the other spatial derivatives in equations (1, 2) are discretised using the standard second order accurate central difference schemes. A central scheme applied to the convection terms in the mixture fraction equation (3) may result in a violation of the extremum principles of the exact equations when the cell Peclet numbers are greater than around 2. However, the mixture fraction must remain bounded between zero and unity if any unphysical values of the density, temperature and species concentrations are to be avoided. In order to achieve this a Total Variation Diminishing (TVD) scheme, Sweby [34], is used for the convective terms in the mixture fraction equation.

The time derivatives in equations (1-3) are approximated by a three point backward difference scheme with a variable time-step to ensure that the maximum Courant number, based on the filtered velocity, always lies between 0.1 and 0.2.. The pressure is determined by a two-step second-order time-accurate approximate factorisation method. A co-located pressure and velocity arrangement is used and an odd/even node uncoupling of the pressure and velocity fields is prevented by a pressure smoothing technique, Rhie and Chow [35]. The

system of the algebraic equations resulting from the discretisation is solved using the matrix pre-conditioned conjugate gradient methods; Bi-CGSTAB [36] for the velocity and scalar equations, and ICCG (1,1,1) [37] for the pressure.

The time mean (average) values, defined as

$$< \tilde{\phi} >= \frac{1}{N} \sum_{n=1}^{N} \tilde{\phi}(x_i, t), \tag{8}$$

have been accumulated over a total of $N = 3 \times 10^5$ time steps, where ϕ is a generic flow variable. The sub-grid contribution to the rms (root mean square) values are negligible and are ignored with the consequence that the rms of turbulence fluctuations in $\tilde{\phi}$ is obtained from

$$\phi'_{rms} = \left(\frac{1}{N} \sum_{n=1}^{N} \left(\tilde{\phi} - < \tilde{\phi} > \right)^2 \right)^{1/2}. \tag{9}$$

4 Results and discussion

In this section we begin with the presentation of the results of the flamelet computations and this is followed by the presentation of the LES results including the flame temperature, density, mixture fraction and species concentrations. Results of the velocity field, and the turbulent fluctuating and sgs quantities are presented thereafter.

4.1 Laminar flamelet calculation

The dependencies of temperature, density and species mass fraction on the mixture fraction (ξ) resulting from the laminar flamelet computations used in the combustion model are presented in Fig. 3. The flamelet is generated

at a strain rate of $15s^{-1}$ and the boundary conditions are taken to comply with the experimental pre-heated conditions for the air [1]. In steady laminar counterflow flames the composition depends on the mixture fraction and the rate of strain, with extinction occurring at high strain rates. However, the incorporation of strain or flame stretch effects into LES is problematic and knowledge of the local rate of strain or the scalar dissipation rate - often used in RANS approaches - is insufficient to characterise local extinction. For this reason a flamelet at a single strain rate is selected and the strain rate below $15s^{-1}$ did not show any significant changes in flame temperature and species concentrations. A detailed reaction mechanism consisting of a total of 87 species and 466 reactions has been used to generate the flamelet data. Further details of the reaction mechanism can be found in Leung [38]. To account for the radiative heat loss to the combustor walls, the flamelet temperature is adjusted using the following relation, Fairweather et al. [39]:

$$T(\xi) = T_{ad}(\xi)\left[1 - \chi\left(\frac{T_{ad}(\xi)}{T_{ad,max}}\right)^4\right], \tag{10}$$

where T_{ad} represents the adiabatic flamelet temperature, and the radiative fraction, χ, which is taken as 0.2, gives good agreement with the measured peak temperature.

In Fig. 3 the temperature of $773K$ at a mixture fraction (ξ) of 0 corresponds to that of the pre-heated air stream, whereas the temperature of $298K$ at $\xi = 1$ is that of the propane. At the stoichiometric condition (ξ_{stoich}), which is at about 0.06, the oxygen and fuel stream curves meet together and react, see in Fig. 3 (iii), as a result a maximum temperature of $1896K$ is achieved at this location of ξ. The corresponding density at stoichiometric shows a minimum value. The concentrations of CO_2 and H_2O have their maximum

close to the stoichiometric condition, whereas the other products have the maximum values under the fuel rich conditions.

4.2 Temperature, density and mixture fraction

In Fig. 4 some snapshots of the instantaneous flame temperature, $\tilde{T}$, on the horizontal midplane of the combustor are plotted at different simulation times for Case1. The purposes of this figure are to visualise the development of flame and its structure by means of the temperature distributions and also to show how the structure of the flame temperature varies with time. At the inlet when the fuel gets its first contact with the air, the combustion takes place and the flame temperature rises. The flame puff, which initially generates near the fuel nozzle, diffuses and propagates towards the downstream of the combustor. A higher colour contour level is seen around the centreline where the combustion occurs around the stoichiometric condition. No combustion occurs near the wall close to the inlet zone where the temperature remains the same as that of the pre-heated air. The mean result in Fig. 5 shows that the flame temperature at the centre of the combustor increases along the axial direction and drops gradually to the downstream from $y \simeq 0.35m$. Moreover, due to the diffusion of the flame the temperature of the walls towards the downstream rises.

In Fig. 6 the computationally predicted mean temperatures, $< \tilde{T} >$, are compared against the measurements of Nishida and Mukohara [1]. The corresponding mean density results are also presented in this figure. In Fig. 6(a), the predicted mean axial temperature on the centreline initially starts with the fuel temperature at the inlet. As the combustion takes place, the flame

temperature increases and achieves a maximum value of $1696K$ (Case1) and $1730K$ (Case2) at about $y = 0.35m$. The flame temperature then drops gradually to the downstream with a value of about $1200K$ (Case1) and 1329 (Case2) arising at the outlet of the combustor. The maximum temperature of $1778K$ at $y = 0.39m$ was recorded in the experiment, which is bit further downstream of our prediction and is slightly under-predicted in the computations. But the peak level of the mean temperature is better predicted in Case2. Moreover, the experimental results show a concave like shape around $y = 0.2m$, which is not evident in the predictions where a slight over-prediction is evident in both the cases. However, overall a very good agreement is achieved and the decaying trend of the temperature along the downstream is also well predicted in Case1. The mean density decreases from the inlet as the temperature rises and becomes minimum at the point where the temperature is maximum. The density then rises very slowly towards the downstream of the combustor, which is consistent with the falling temperature.

The radial distribution of the mean temperature in Fig. 6(b-e) shows that the peak value is slightly under-predicted in the computations and moves towards the wall near the inlet (frames b, c), and the temperature at the centre shows slight over-prediction in both the Cases. In the most downstream stations, in frames (d, e), a slight under-prediction of the temperature occurs at the centre but a better prediction is found in Case2. Despite this slight over and under-prediction of the temperature comparing with the experiment, it is clear that the trend of increasing and decaying of the temperature in the radial direction is matched reasonably well with the experimental data and qualitatively their agreement is good. The radial distributions of the mean temperature predicted by Fairweather et al. [39] using the κ-ϵ turbulence model show an

under-prediction near the inlet (in frames b, c) and over-prediction at the further downstream (in frames d, e). However, comparing the radial temperature profiles against the experimental measurements, the predicted results in the present computations have some better agreement in frames (d, e). Again the mean density shows minimum values at the locations of the maximum temperature as the mean density of the mixture is inversely proportional to the temperature.

It might be interesting to see how the results presented above are linked with the mixture fraction and its sub-grid scale variance, given the fact that they are a function of these two variables. These results are presented in Fig. 7. The rapid decay of the mixture fraction in the upstream region from its highest level at the inlet corresponds to the 'fast' mixing with the supplied air stream. The mixture fraction in both Case1 and Case2 is found almost same at the upstream, but towards the downstream of the combustor, where it decays slowly, is predicted slightly higher in Case2. However, in both the cases, a very good agreement is shown with the experimental data of Nishida and Mukohara [1]. The magnitude of the sub-grid scale variance of the mixture fraction is predicted small and it behaves in the similar way as the mixture fraction, i.e., a rapid decay at the upstream and then slowly decay to the downstream. The radial profiles of the mixture fraction and the sgs variance also show clearly that the curve drops gradually with y and that it diffuses towards the wall. The dotted straight line in frames (a, b) indicates the location of the stoichiometric mixture fraction in the computation.

4.3 Combustion species

In Figs. 8-10, comparisons of the predicted species mean mole fractions with those of the experiment are made. The centreline mean mole fraction of C_3H_8 in Fig. 8(a) decays rapidly, which is consistent with the fast decay of the mixture fraction profile seen in Fig. 7(a), and has an excellent agreement with the experimental data. The mole fraction of N_2 is predicted very well in the downstream, while the reactant O_2 is well predicted against the experiment at the upstream with an over-prediction at the downstream region. The experimental results of O_2 show hardly any variation from the mid-location of the combustor, whereas in the simulations O_2 increases continuously towards the downstream, a result that is consistent with the simulated mixture fraction decay (Fig. 7) and the flamelet data shown in Fig. 3. Note that Fairweather et al. [39] had an under-prediction of O_2 throughout the centerline.

The peaks of the combustion products CO and H_2 are over-predicted compared with the experiment but the trends are well reproduced. The mole fraction of CO_2 is well-predicted up to $y = 0.3m$ but shows an under-prediction beyond this region. The mole fraction of H_2O is over-predicted within the region of $0.28m < y < 0.7m$ and is under-predicted near the inlet and outlet regions. The products of the two unburned hydrocarbons, C_2H_2 and CH_4, are compared in frames (h, i). The peaks of C_2H_2 show an under-prediction, however, the flamelet data in Fig. 3 clearly shows that the peak value of C_2H_2 would not exceed the maximum limit of about 0.025 when the mixture fraction variance is close to zero. The peak level of C_2H_2 obtained by Fairweather et al. [39] is also under-predicted, but comparatively better than the present results. CH_4 is slightly over-predicted up to $y = 0.1m$ but is well-predicted in

the rest of the domain.

The radial plots in Figs. 9, 10 show that the trends in which the species curves grow or decay along the radial direction compare well with the experiment and comply well with the flamelet data. The over-prediction of the peaks in some species, e.g. CO and H_2 in Fig. 9; and the under-prediction of the peaks in H_2O and C_2H_2 in Fig. 9, and CO_2 and C_2H_2 in Fig. 10 might be linked with the uncertainties in the reaction mechanisms (Leung et al. [40]) used to generate the flamelets, which particularly concern the formation of a number of minor species in the propane flame. We also note that no comparison was possible to make for C_3H_8 at $y = 0.3m$ due to the absence of the experimental data.

4.4 Velocity field

Fig. 11 shows that the level of fluctuations in the instantaneous velocity components and pressure at the downstream of the inlet is much higher compared to the rest of the domain, and these fluctuations slowly decay towards the downstream. The mean axial velocity, $< \tilde{v} >$, also decays from its maximum at the inlet towards the downstream but varies a little when $y > 0.3m$. The profile behaves like a fully developed flow established from about the one-third axial location of the combustion chamber where the gradient of the centreline velocity, $\frac{\partial < \tilde{v} >}{\partial y}$, tends to zero. That is why, in this figure and the rest of figures where the axial results are plotted, the data are plotted up to the maximum axial location of $0.35m$ in order to clearly view the results of the velocity and turbulent characteristics which are dominant mostly at the upstream region.

The power law profile for the centreline mean axial velocity of an axisymmetric turbulent fully developed flow, which is approximated by using $\frac{<\tilde{v}>}{<\tilde{v}>_{y=0}} = 6.4\left(\frac{y}{D}\right)^{-n}$, Tennekes and Lumley [41], where the index n takes a value of unity and D is the internal diameter of the fuel nozzle, is plotted in Fig. 11(b) as a solid line with circles in order to get a qualitative feeling of the mean axial velocity achieved in the simulations. It clearly shows that the trend is same though we don't expect that these results would match perfectly with the power law fittings, this is simply due to the case of combustion where the results are affected by the many factors such as the density field which varies in the simulation and the pressure which is coupled with the combustion temperature. The choice of the dynamic sub-grid scale model makes no difference in the mean velocity and pressure profiles, and the deep mean-pressure drop after the inlet occurs due to the temperature and density variation between the fuel and air.

4.5 Turbulent fluctuating and sgs quantities

In Fig. 12 the centreline profiles of the mean turbulent shear stresses are presented. The high level of the turbulent shear stresses found at the upstream plays an important role in determining the mean flow as they contribute to a large amount of momentum transfer in the flow. The rms results of the fluctuating components in Fig. 13 show a sharp rise from the inlet and achieve their peak where the magnitude of the stresses is high. The rms then drop gradually towards the downstream, and a very little variation is shown in the further downstream. Comparing between the results of the two sgs models, samll variations in the stresses and rms are found at the upstream of the

combustor.

The mean mixture fraction fluxes along the centreline are depicted in Fig. 14, which again show that the magnitude of the fluxes is high at the upstream because of the turbulent fluctuation. Note that these fluxes play a dominant role in the mixing of air and fuel together and also contribute to the scalar transports. Moreover, the mixture fraction flux with the axial velocity component, $< v'\xi' >$, has the largest value compared to the other two fluxes as the axial velocity is higher than that of the radial components. Similar to the resolved scale stresses, the magnitude of the fluxes decreases towards the downstream as the intensity (rms) of the turbulence is predicted very low there, and the two sgs models show some variations at the upstream, but small.

In Figs. 15 and 16, the mean centerline values of the sub-grid scale shear stresses and the sub-grid scale mixture fraction fluxes are presented respectively. The sub-grid scale contributions to the shear stresses and the mixture fraction fluxes are predicted maximum at the upstream since the turbulent intensity found was high here. The sgs contributions are negligible and almost vanish beyond the region of $y = 0.1m$ of the combustor. The effects of the two sgs models on the sub-grid scale quantities are now evident in Figs. 15 and 16 which show that Case2 (dynamics sgs model) gives higher values of the sgs stresses and fluxes in the upstream where the dynamic value of C_s found is higher than 0.1.

5 Conclusion

Large Eddy Simulation technique has been applied to investigate the turbulent flow, species concentration and temperature arising in the turbulent non-premixed combustion of propane-air in a cylindrical combustor. The conserved scalar approach with the laminar flamelet model is used to the modelling of the combustion process. The LES results are obtained by employing the Smagorinsky model with a constant C_s of 0.1 as well as the dynamically calibrated C_s.

The predicted mean temperature and species concentration in both the axial and radial directions have been compared with those of the experimental data obtained by Nishida and Mukohara [1] in the turbulent propane and pre-heated air combustion. The mean temperature and mixture fraction predictions show very good agreement with the experimental data, while some combustion species at some locations are under or over predicted in the computations. The possible reasons of these have been discussed in the paper, which involves some of the uncertainties in the reaction mechanisms (Leung et al. [40]) used to generate the flamelets for this study. Moreover, the simplified treatment of the radiative heat loss from the flame might have some effects on the prediction of temperature and species concentration. A full coupling of LES with a radiation model is required to better account the radiative heat loss and the effects of these on the species concentrations. However, this clearly involves significant challenges in the development of subgrid scale interactions between the combustion and radiation and would deserve significant computing resources as well. Furthermore, in the experimental study of Nishida and Mukohara [1], a small part of the fuel was injected through the annular sur-

rounding to form a pilot flame. This has been ignored in our computations as no detailed information was available in the experimental paper on the pilot flame nozzle and the fuel flow rate through it. It is possible that including the pilot flame in the simulations might have resulted in some of the species and temperature profiles being in closer agreement with the experimental data.

Most of the results are almost uninfluenced by the choice of the sub-grid scale models, whether it is a Smagorinsky model with constant C_s of 0.1 or a dynamic model for C_s. However, the mean mole fraction of O_2 is predicted better in the dynamic model, which in turn leads to a slightly better prediction in CO_2 and H_2O by this model. It is also found that the sub-grid scale quantities are predicted higher by the dynamic model in the upstream region where the value of dynamic C_s is found higher than the constant C_s of 0.1.

In the fuel nozzle exit of the combustor, combustion occurred under the fuel-rich conditions where the overall equivalence ratio was 0.6, which produced various forms of hydrocarbons in the combustion products. One of them is acetylene, C_2H_2, which usually contributes to the formation and growth of soots (solid carbon particles, solid emissions) in the combustion process. Research is currently underway in order to predict the soot formation and growth in the same flame.

Acknowledgement

The first author thanks to the Faculty of Engineering of the University of Glasgow for a postgraduate studentship.

References

[1] O. Nishida, S. Mukohara, Characteristics of soot formation and decomposition in turbulent diffusion flames, Combustion and Flame 47 (1982) 269–279.

[2] O. Reynolds, On the dynamical theory of incompressible viscous fluids and the determination of the criterion, Phil. Trans. of the Royal Society of London 86(Series A) (1895) 123–164.

[3] L. Vervisch, T. Poinsot, Direct Numerical Simulation of Non-Premixed Turbulent Flames, Annual Review of Fluid Mechanics 30 (1998) 655–691.

[4] J. Smagorinsky, General circulation experiments with the primitive equations I. The basic experiment, Monthly Weather Review 91(3) (1963) 99–164.

[5] D. K. Lilly, The representation of small-scale turbulence in numerical simulation experiments, in: Proc. IBM Scientific Computing Symposium on Environmental Science, N.Y., 1967, pp. 195–210.

[6] J. W. Deardorff, A numerical study of three-dimensional turbulent channel flow at large Reynolds numbers, J. Fluid Mech.. 41(2) (1970) 453–480.

[7] K. Akselvoll, P. Moin, Large-eddy simulation of turbulent confined coannular jets, J. Fluid Mech. 315 (1996) 387–411.

[8] W. P. Jones, M. Wille, Large-eddy simulation of a plane jet in a crossflow, Int. J. Heat and Fluid Flow 17 (1996) 296–306.

[9] L. L. Yuan, R. L. Street, J. H. Ferziger, Large-eddy simulations of a round jet in a crossflow, J. Fluid Mech. 379 (1999) 71–104.

[10] L. di Mare, W. P. Jones, LES of turbulent flow past a swept fence, Int. J. Heat and Fluid Flow 24 (2003) 606–615.

[11] M. Lesieur, O. Metais, New Trends in Large-Eddy Simulations of Turbu-

lence, Annual Review of Fluid Mechanics 28 (1996) 45–82.

[12] P. Moin, Progress in Large Eddy Simulation of Turbulent Flows, Tech. rep., AIAA 97-0749 (1997).

[13] M. Lesieur, O. Metais, P. Comte, Large-Eddy Simulations of Turbulence, Cambridge University Press, 2005.

[14] F. Gao, E. E. O'Brien, A large-eddy simulation scheme for turbulent reacting flows, Phys. Fluids A 5(6) (1993) 1282–1284.

[15] P. E. DesJardin, H. Frankel, Large eddy simulation of a nonpremixed reacting jet: Application and assessment of subgrid-scale combustion models, Phys. Fluids 10(9) (1998) 2298–2314.

[16] N. Branley, W. P. Jones, Large Eddy Simulation of a Turbulent Nonpremixed Flame, Combustion and Flame 127 (2001) 1914–1934.

[17] F. di Mare, W. P. Jones, K. R. Menzies, Large Eddy Simulation of a model gas turbine combustor, Combustion and Flame 137 (2004) 278–294.

[18] W. P. Jones, S. Navarro-Martinez, Large Eddy Simulation of Autoignition with a sub-grid Probability Density Function Method, Combustion and Flame 150 (3) (2007) 170–187.

[19] W. P. Jones, S. Navarro-Martinez, Study of hydrogen auto-ignition in a turbulent air co-flow using a Large Eddy Simulation approach, Computers and Fluids 37 (7) (2008) 802–808.

[20] N. Peters, Turbulent Combustion, Cambridge University Press, 2000.

[21] H. Pitsch, Large-Eddy Simulation of Turbulent Combustion, Annual Review of Fluid Mechanics 38 (2006) 453–482.

[22] J. J. Riley, Review of Large-Eddy Simulation of Non-Premixed Turbulent Combustion, Journal of Fluids Engineering.

[23] A. Leonard, Energy cascade in large-eddy simulations of turbulent fluid flows, Advances in Geophysics 18(A) (1974) 237–248.

[24] A. Favre, Statistical equations of turbulent gases, in: Problems of Hydrodynamics and Continuum Mechanics, Tech. rep., Society of Industrial and Applied Mathematics, Philadelphia (1969).

[25] M. Germano, U. Piomelli, P. Moin, W. H. Cabot, A Dynamic Subgrid-Scale Eddy Viscosity Model, Physics of Fluids A 3(7) (1991) 1760–1765.

[26] A. Yoshizawa, Eddy-Viscosity-Type Subgrid-Scale Model with a Variable Smagorinsky Coefficient and its Relationship with the One-Equation Model in Large Eddy Simulation, Physics of Fluids A 3 (1991) 2007–2009.

[27] H. Schmidt, U. Schumann, Coherent structure of the convective boundary layer derived from large-eddy simulations, J. Fluid Mech. 200 (1989) 511–562.

[28] N. Peters, Laminar diffusion flamelet models in non-premixed turbulent combustion, Prog. Energy Combust. Sci. 10 (1984) 319–339.

[29] R. W. Bilger, Turbulent flows with nonpremixed reactants, In P. A. Libby and F. A. Williams, editors, Turbulent Reactings Flows, chapter 3 (Springer-Verleg, Heidelburg, 1980) 65–113.

[30] S. C. Paul, Large Eddy Simulation of a Fuel-Rich Turbulent Non-Premixed Reacting Flow With Radiative Heat Transfer, Department of Mechanical Engineering, University of Glasgow, (2008) PhD thesis.

[31] F. Durst, B. Unsal, Forced laminar-to-turbulent transition of pipe flows, J. Fluid Mech. 560 (2006) 449–464.

[32] J. Laufer, The Structure of turbulence in fully developed pipe flow, Tech. rep., NACA report 1174 (1953).

[33] Y. Morinishi, Conservation properties of finite difference schemes for incompressible flow, Center for Turbulence Research, (1995) 121–132.

[34] P. Sweby, High resolution schemes using flux limiters for hyperbolic conservation laws, SIAM J. Numer. Anal. 21(5) (1984) 995–1011.

[35] C. M. Rhie, W. L. Chow, Numerical study of the turbulent flow past a airfoil with trailing edge seperation, AIAA Journal 21(11) (1983) 1525–1532.

[36] H. A. Van der Vorst, BI-CGSTAB: A fast and smoothly converging variant of BI-CG for the solution of nonsymmetric linear systems, SIAM J. Sci. Stat. Compt. 13(2) (1992) 631–644.

[37] D. S. Kershaw, The complete Cholesky-conjugate gradient method for the iterative solution of systems of linear equations, Journal of Cmputational Physics 26 (1978) 43–65.

[38] K. M. Leung, Kinetic modelling of hydrocarbon flames using detailed and systemically reduced chemistry, Department of Mechanical Engineering, Imperical College London, (1995) PhD thesis.

[39] M. Fairweather, W. P. Jones, H. S. Ledin, R. P. Lindstedt, Predictions of soot formation in turbulent, non-premixed propane flames, in: 24th Symposium (International) on Combustion / The Combustion Institute, 1992, pp. 1067–1074.

[40] K. M. Leung, R. P. Lindstedt, W. P. Jones, A simplified reaction mechanism for soot formation in non-premixed flames, Combustion and Flame 87 (1991) 289–305.

[41] H. Tennekes, J. L. Lumley, A First Course in Turbulence, The MIT Press, 1972.

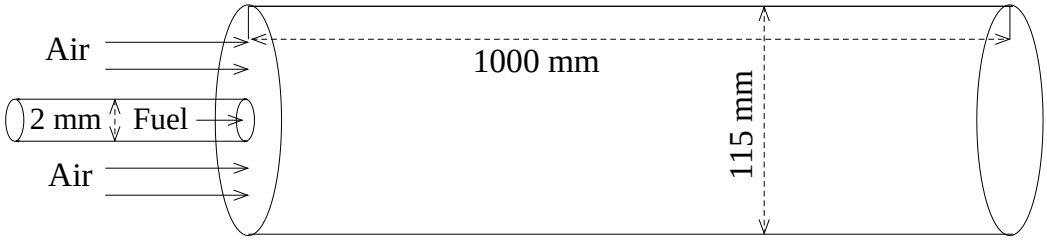

Fig. 1. A schematic of the cylindrical combustor with computational domain.

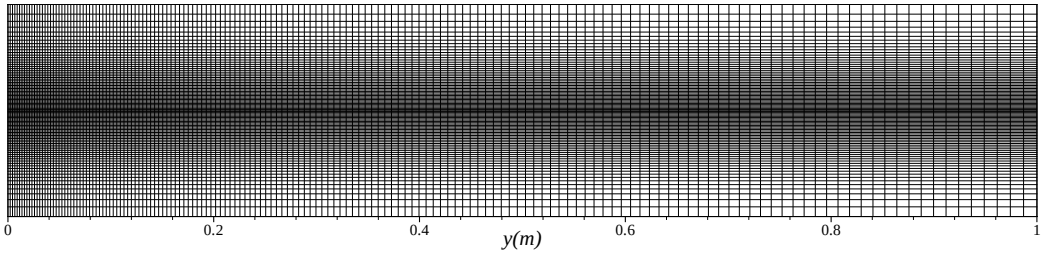

Fig. 2. Mesh distribution showing in the horizontal midplane of the combustion chamber.

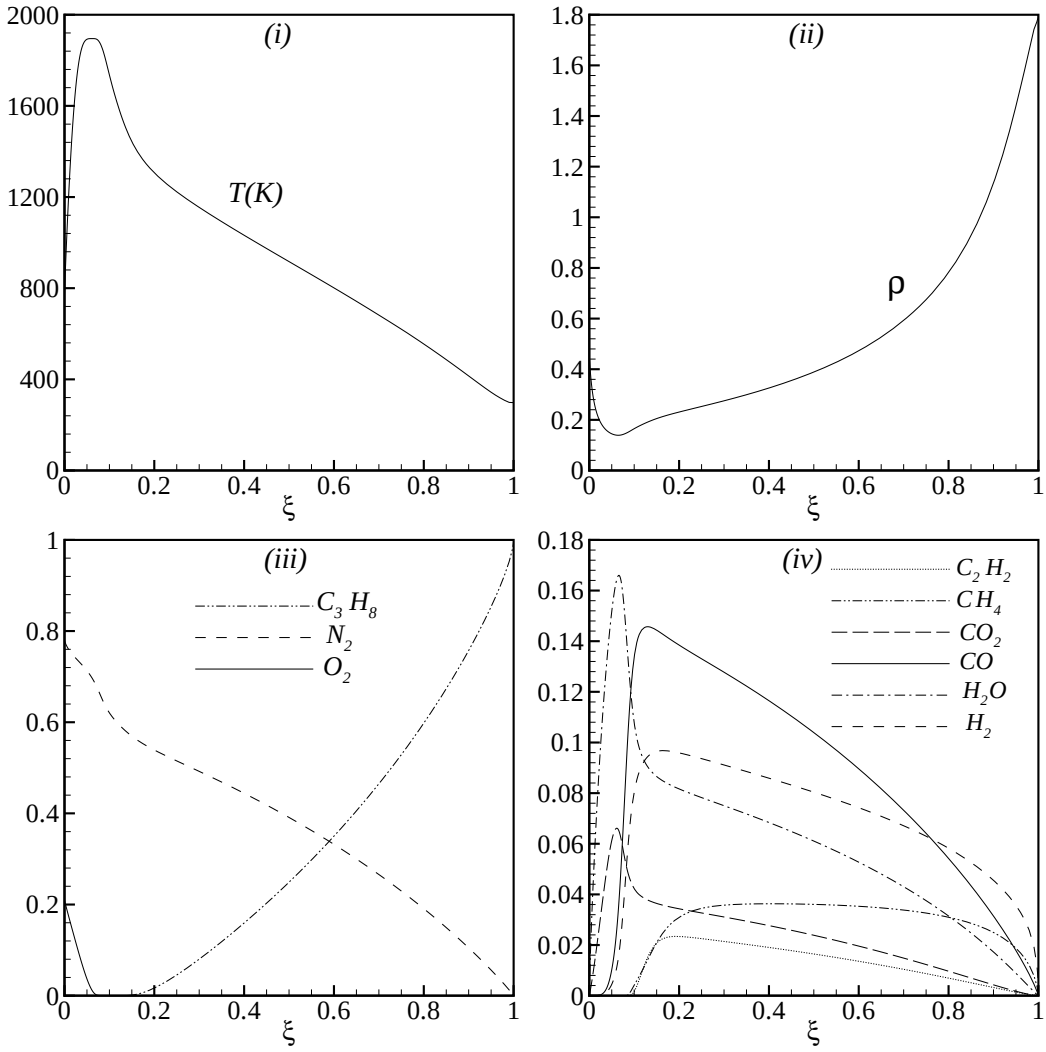

Fig. 3. Laminar flamelet results showing the dependence of the (i) temperature, (ii) density and (iii)-(iv) species mole fractions on the mixture fraction.

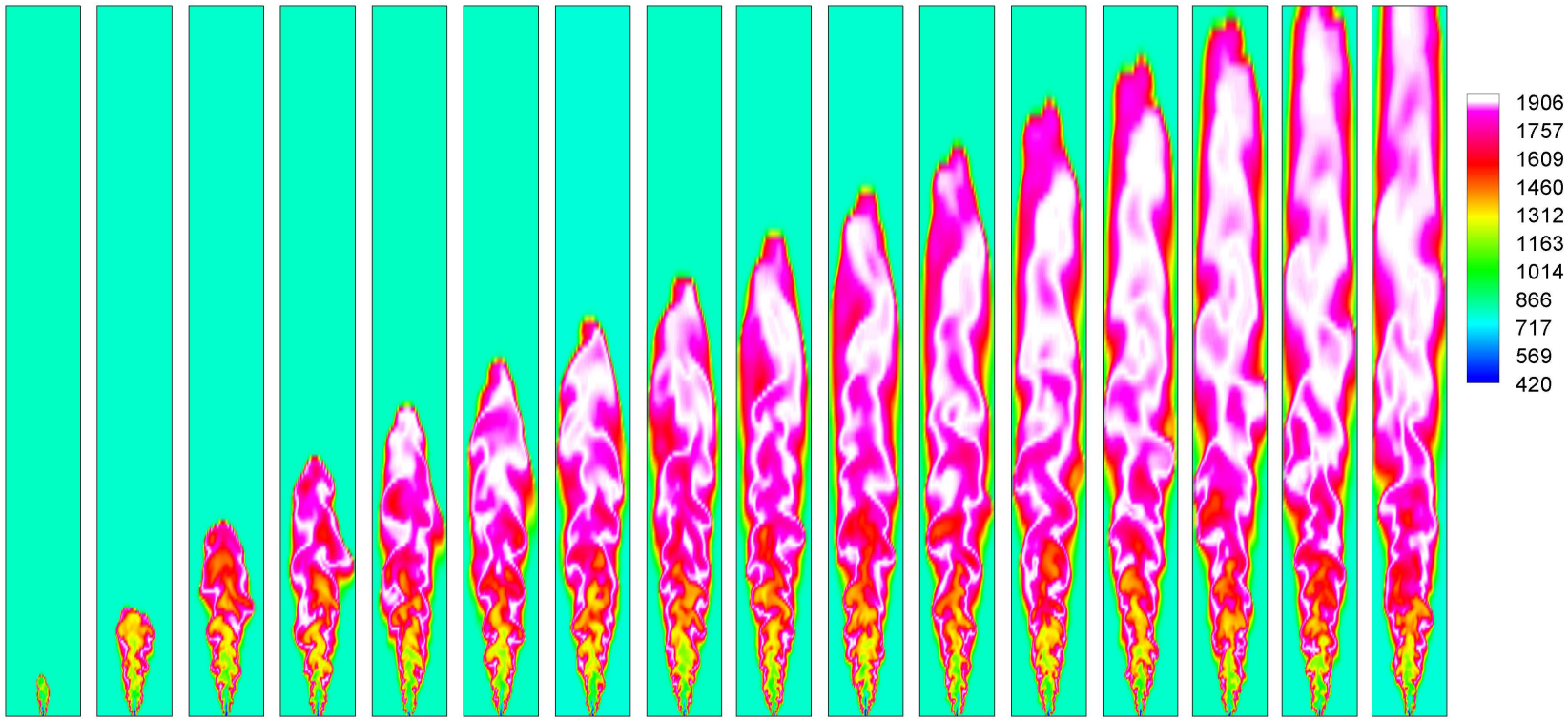

Fig. 4: Instantaneous temperature plots on the horizontal midplane of the combustor for Case1 at (left to right) $t = 3.6 \times 10^{-3}$, 2.86×10^{-2}, 6.31×10^{-2}, 9.13×10^{-2}, 1.17×10^{-1}, 1.43×10^{-1}, 1.69×10^{-1}, 1.96×10^{-1}, 2.22×10^{-1}, 2.48×10^{-1}, 2.74×10^{-1}, 3.01×10^{-1}, 3.26×10^{-1}, 3.51×10^{-1}, 3.76×10^{-1}, and 4.01×10^{-1} sec.

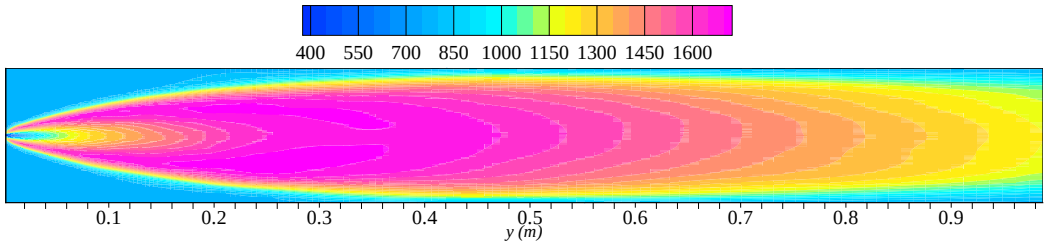

Fig. 5. Mean temperature plot on the horizontal midplane of the combustor for Case1.

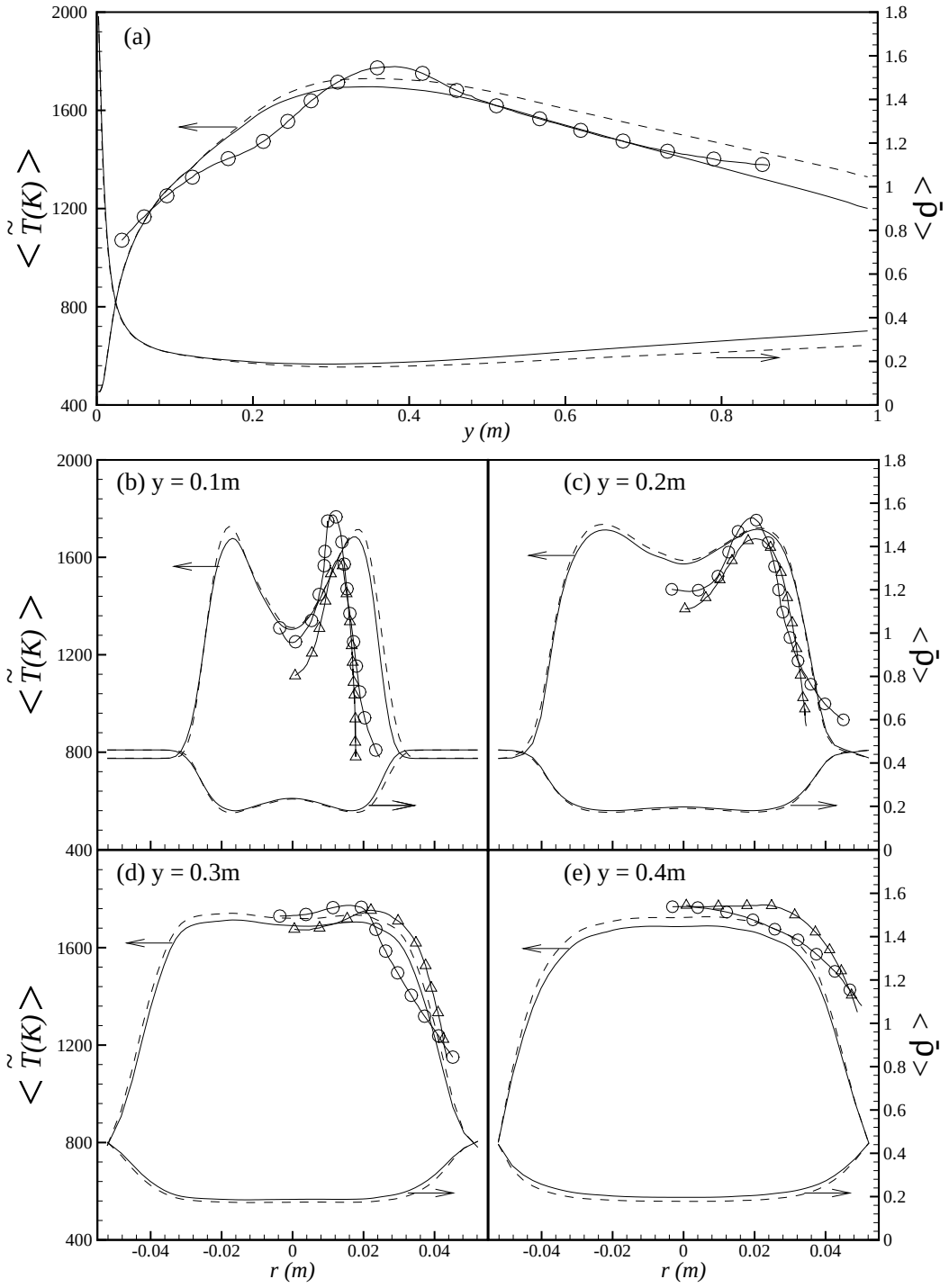

Fig. 6. Comparisons of the mean temperature results with those of the experimental data; (a) the centreline data; and (b-e) the radial data at different cross-sectional positions. Solid line, Case1; Dashed line, Case2; Solid line with circles, experiment [1]; Solid line with triangles, Fairweather et al. [39].

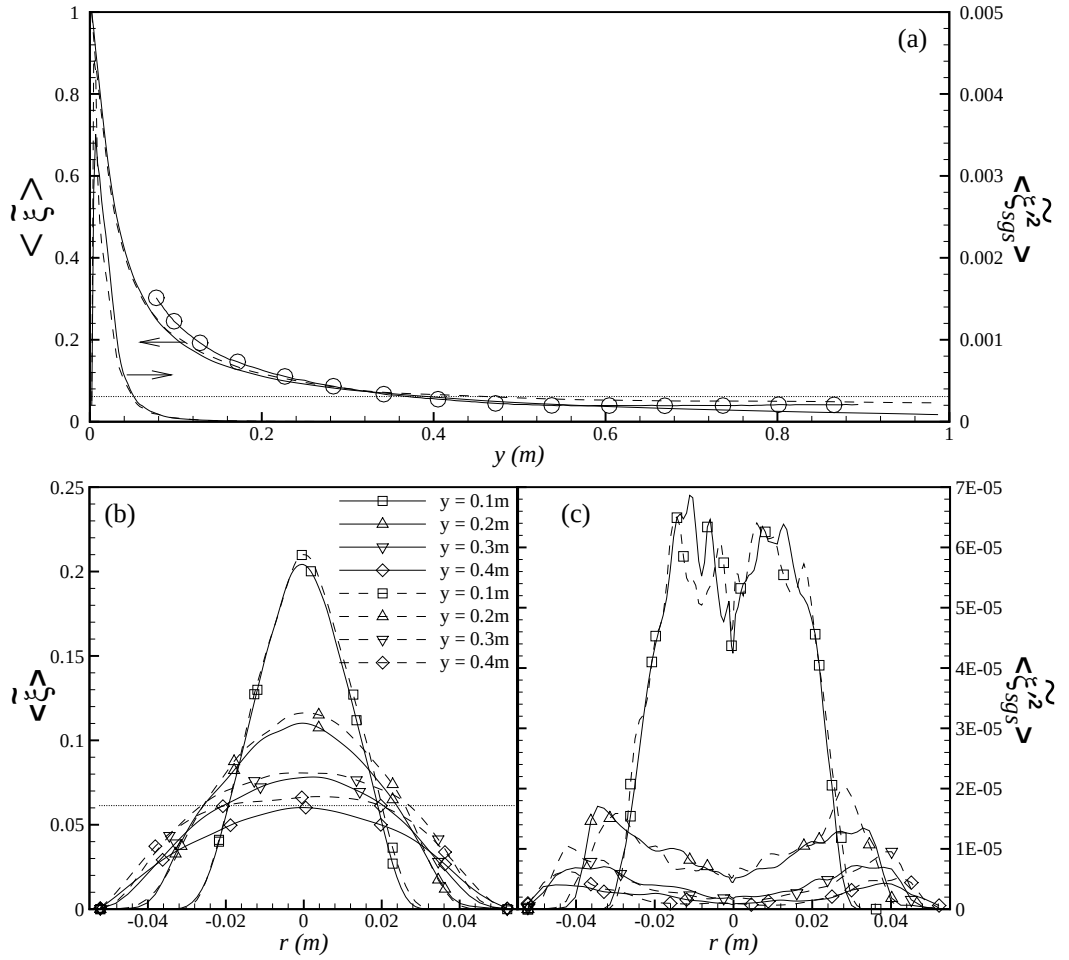

Fig. 7. Profiles of the mixture fraction and its variance along (a) the axial direction, and (b-c) the radial direction at various cross sections. Solid line, Case1; Dashed line, Case2; Solid line with circle, experiment [1]. The horizontal dotted line in frames (a, b) indicates the location of the stoichiometric mixture fraction.

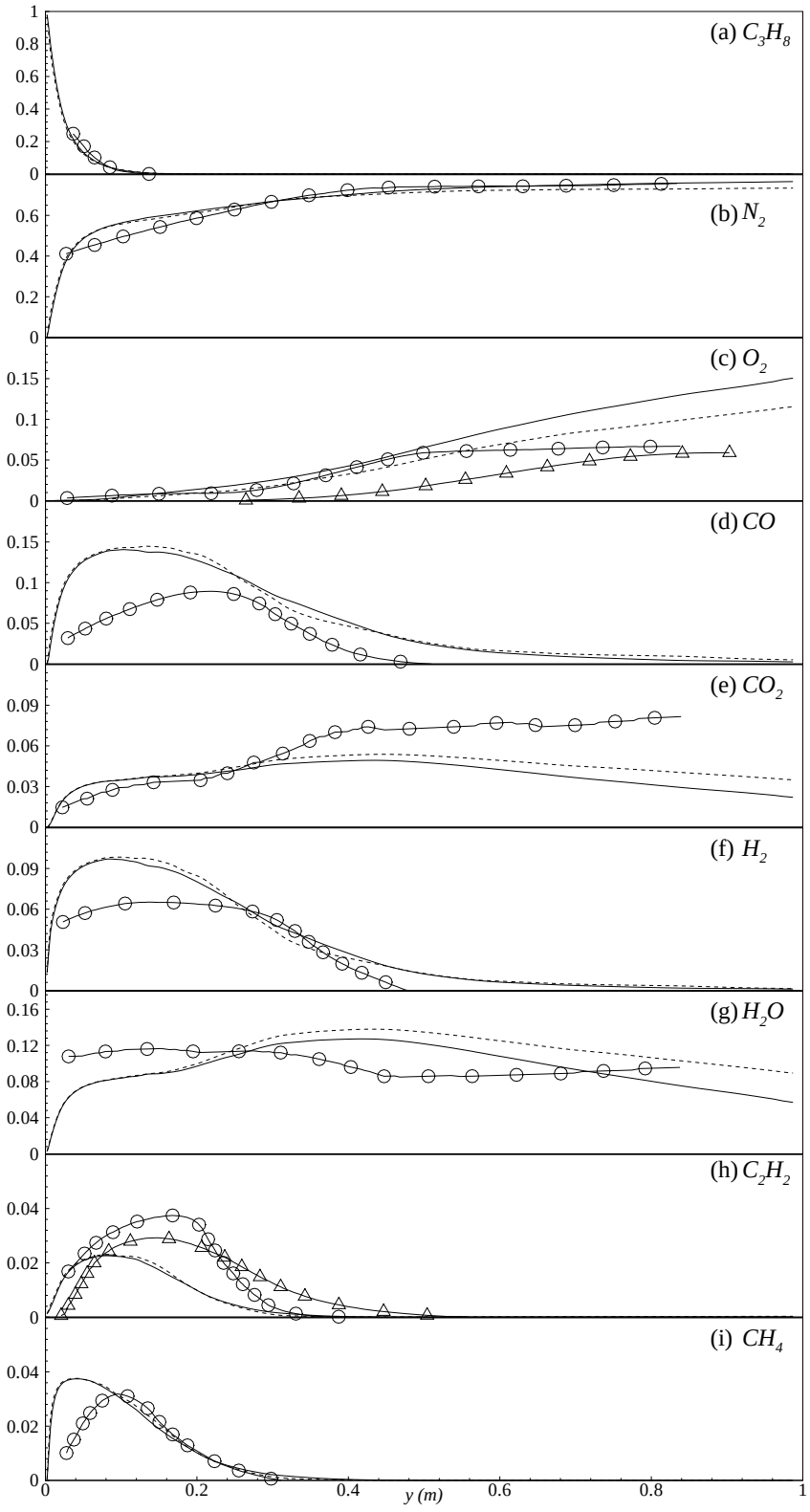

Fig. 8. Mean mole fraction of the combustion species at the centreline. Solid line, Case1; Dashed line, Case2; Solid line with circles, experiment [1]; Solid line with triangles, Fairweather et al. [39].

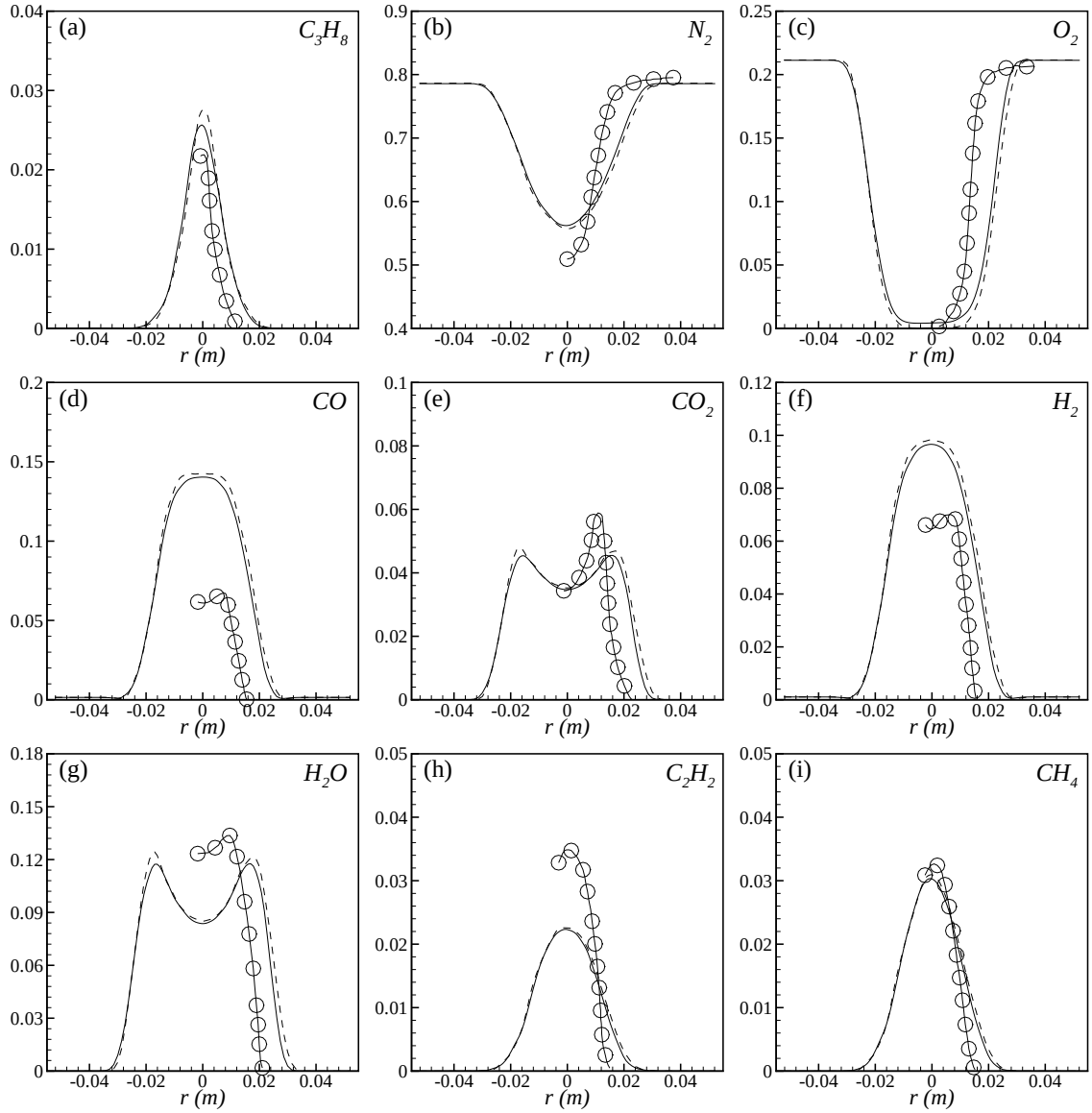

Fig. 9. Mean mole fraction of the combustion species at $y = 0.1m$. Solid line, Case1; Dashed line, Case2; Solid line with circle, experiment [1].

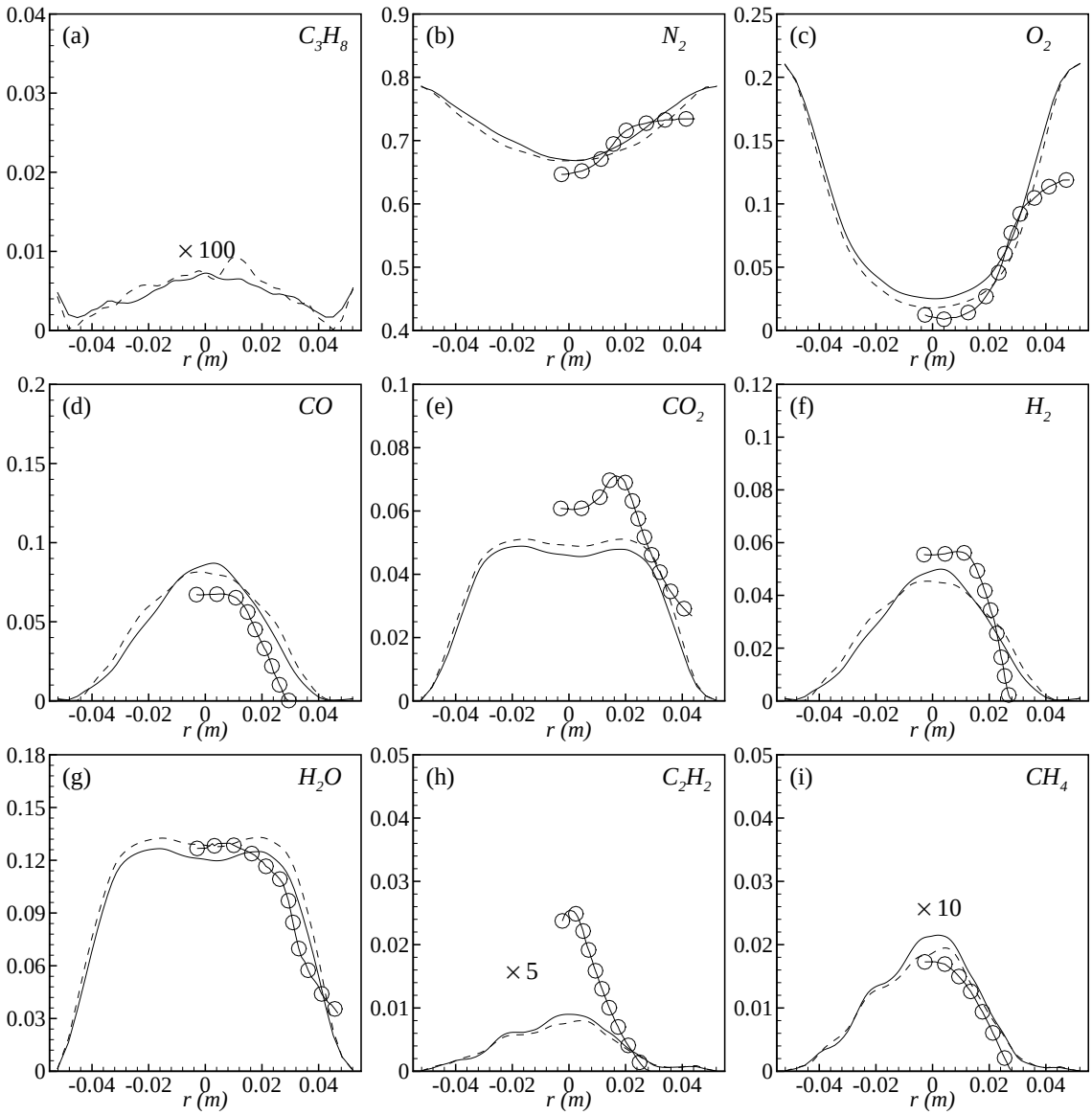

Fig. 10. Mean mole fraction of the combustion species at $y = 0.3m$. Solid line, Case1; Dashed line, Case2; Solid line with circle, experiment [1].

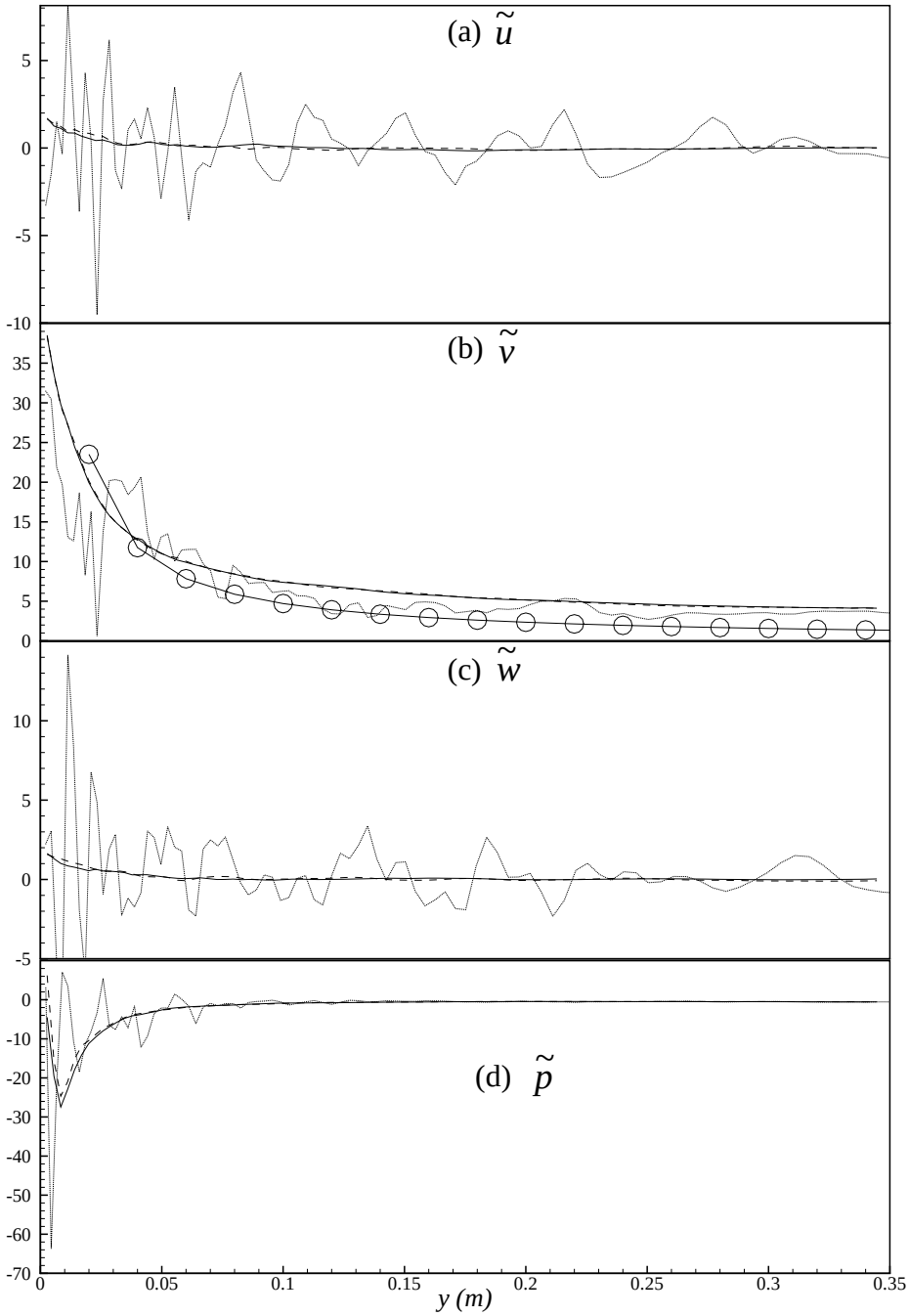

Fig. 11. Centerline profiles of the velocity components (ms^{-1}) and pressure (Pa). Solid line, time mean (Case1); Dashed line, time mean (Case2); Dotted line, instantaneous Favre averaged (Case1); Solid line with circle, mean axial velocity of an axisymmetric fully developed turbulent flow.

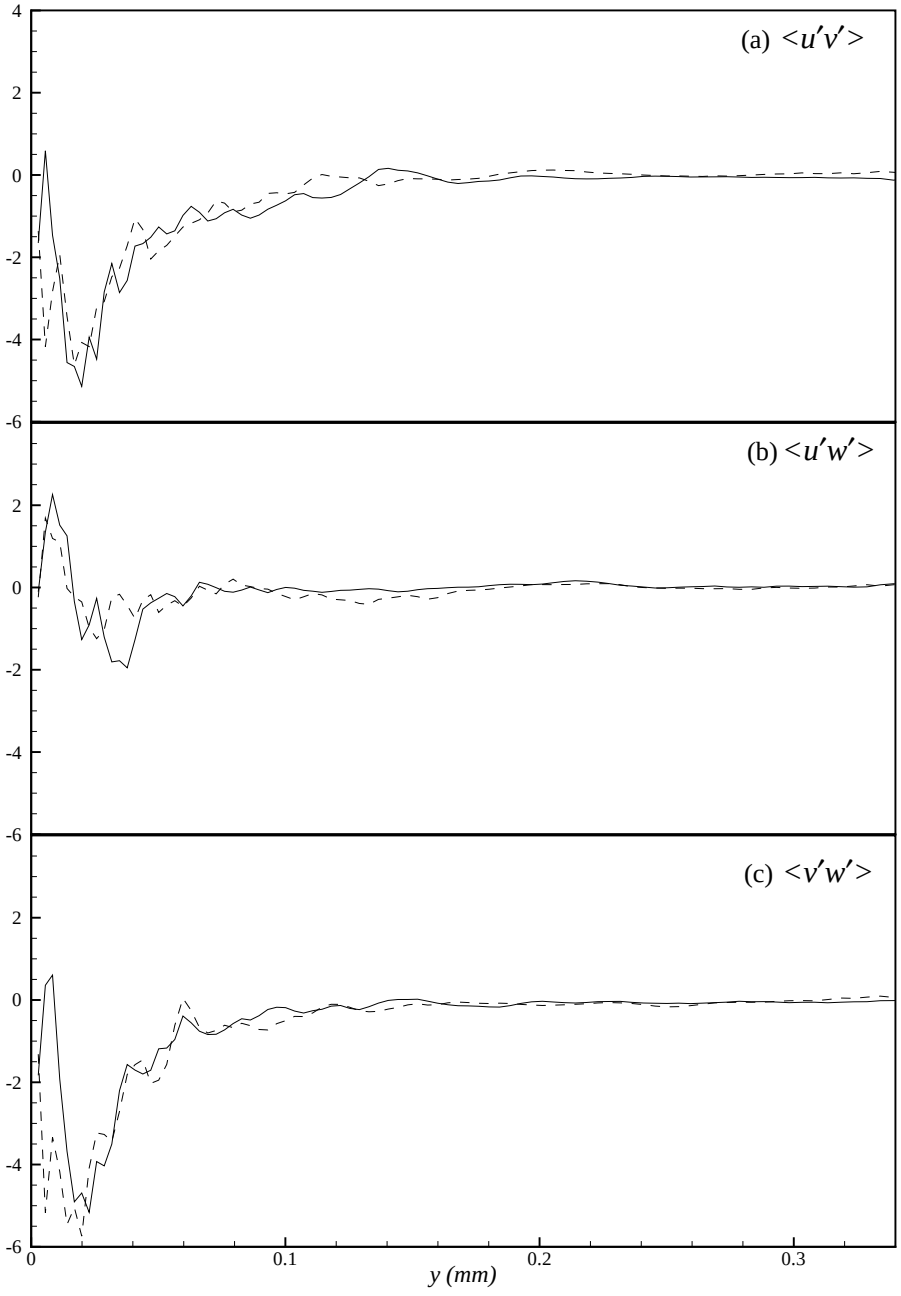

Fig. 12. Centreline profiles of the mean turbulence shear stresses. Solid line, Case1; Dashed line, Case2.

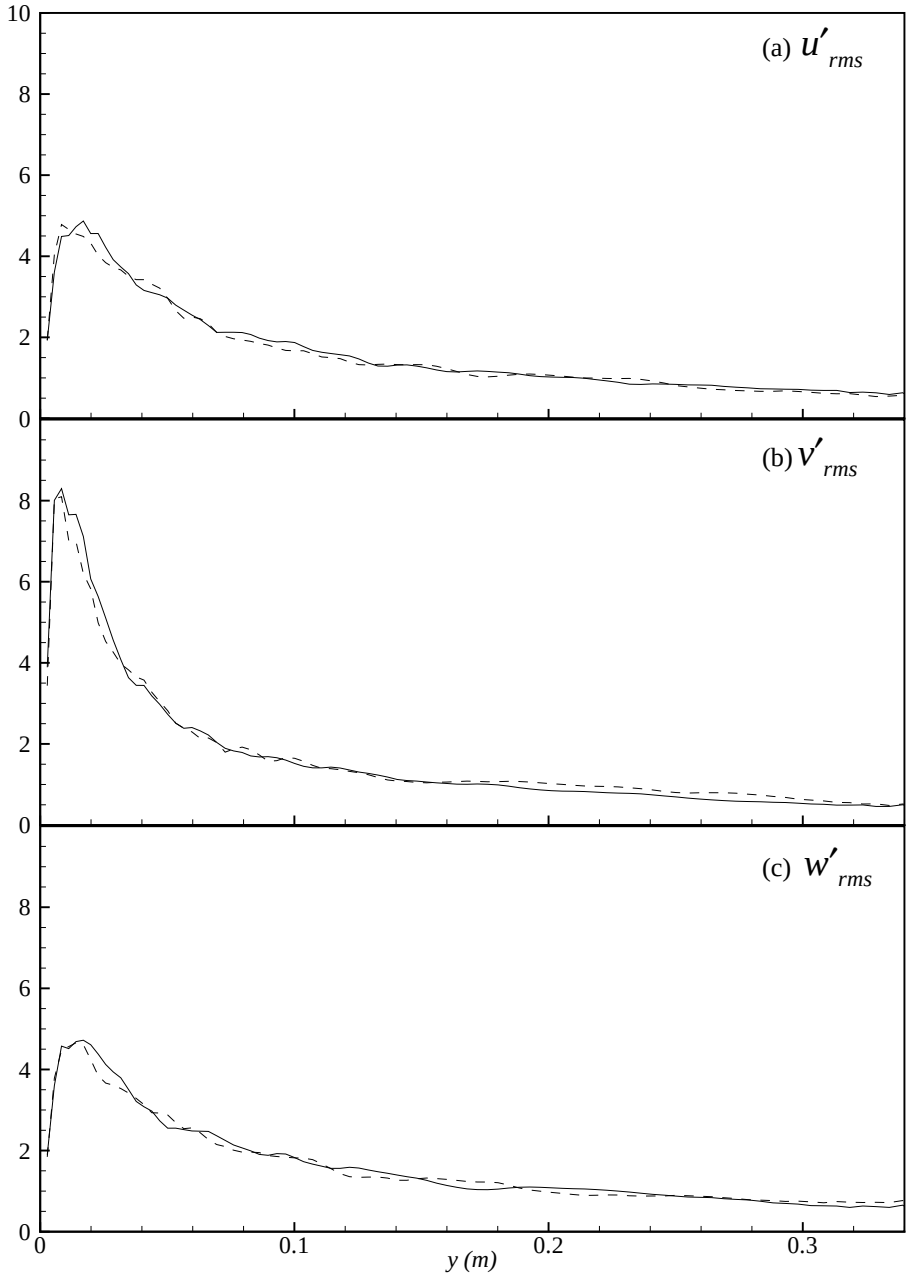

Fig. 13. Root mean square (rms) of the fluctuations, u', v', w', at the centreline. For legend see Fig. 12.

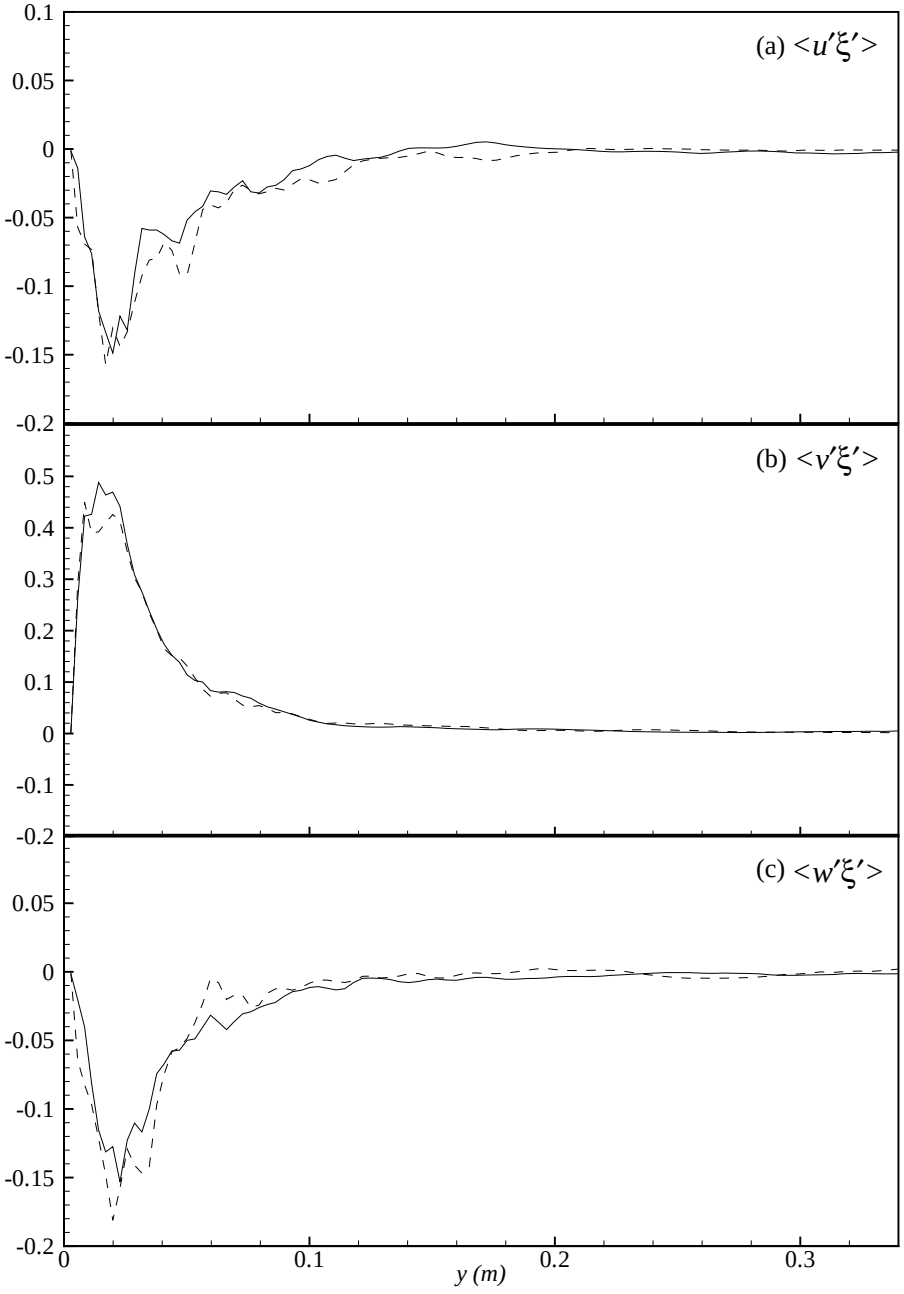

Fig. 14. Centreline profiles of the mean mixture fraction fluxes. For legend see Fig. 12.

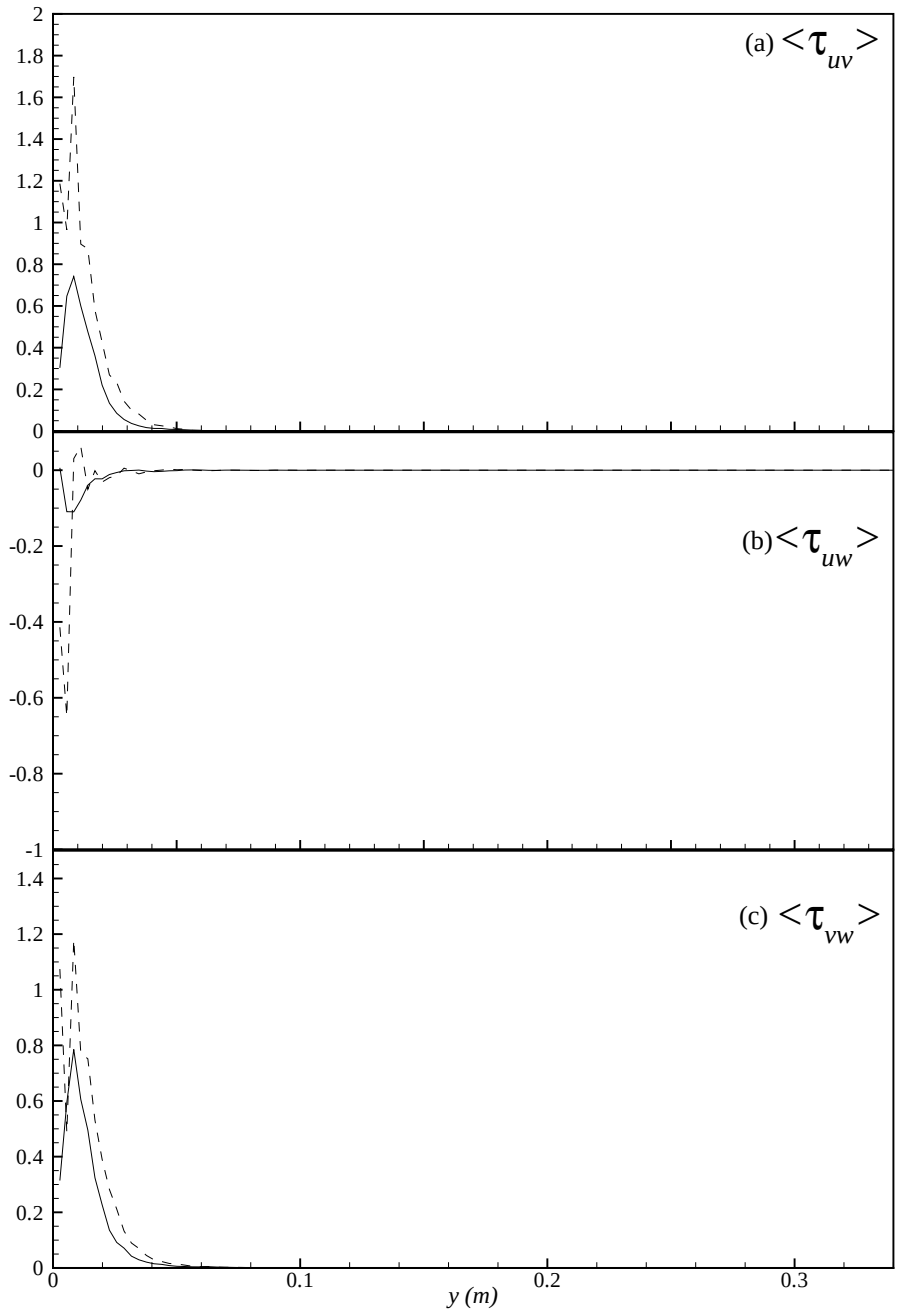

Fig. 15. Centreline profiles of the mean sub-grid scale shear stresses. For legend see Fig. 12.

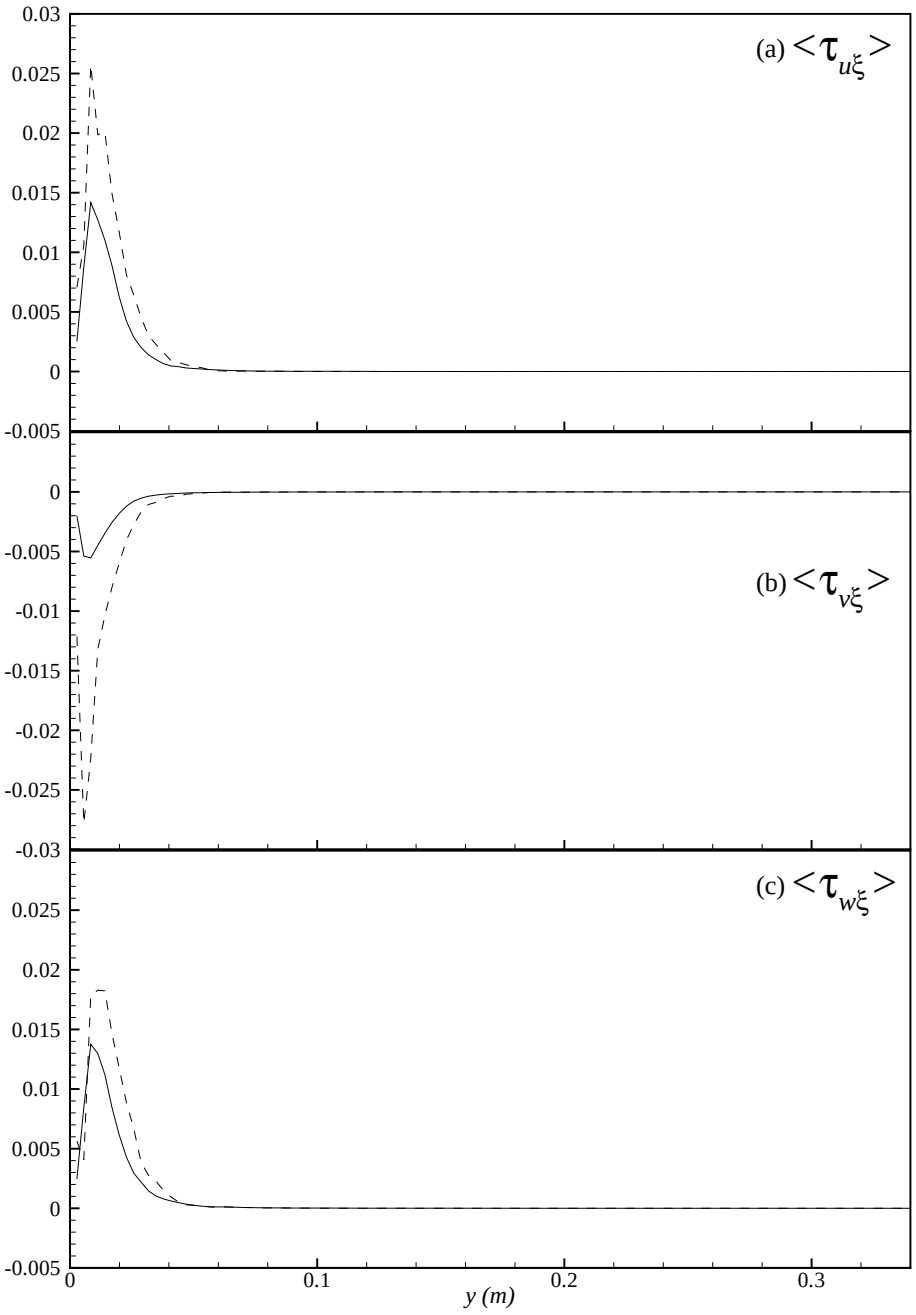

Fig. 16. Centreline profiles of the mean sub-grid scale mixture fraction fluxes. For legend see Fig. 12.